Viscous friction measurement technique in robot joint with the use of surrogate mass

Jerzy Świder, Adrian Zbilski

Faculty of Mechanical Engineering, The Silesian University of Technology

Abstract: This paper is the theoretical analysis of the method for determining viscous friction characteristics in an industrial robot joint. For the purpose of calculating the value of viscous friction, the surrogate mass of driven robot arms and their common surrogate center of gravity was used. In order to ensure the value of surrogate mass to be correct, the analysis of friction hysteresis influence on a motor's driven torque was performed. The analysis of dynamic phenomenon of friction was performed by numerical robot joint and robot arms models.

Keywords: measurements, friction, robot joint, surrogate mass

1. Introduction

The determination of viscous friction characteristics in an industrial robot joint belongs to the dynamic parameters identification process of an investigated plant. However, the measurement of friction in robot joints can not be performed directly using external sensors, due to the lack of sufficient quantities of a place needed for this purpose. Robot arms are designed to be a compact set of many parts. The plant used to analyze the friction measurement technique was the industrial robot FANUC AM100iB. In these types of machines, an accurate model of friction has great importance due to the quality of positioning. Therefore, to model the friction in robot joints a lot of different mathematical friction models were developed. Friction model may be divided into three groups [1]: *white-box*, *black-box*, and g*ray-box*. White-box models are developed based on physical backgrounds of an investigated phenomenon, black-box models are based on an experimental data and application of general models or neural networks and fuzzy logic. On the other hand, the gray-box represents attributes of both previous groups. White-box models are divided into static and dynamic. All of the friction models may be used when ensuring criteria that have to be obtained in the performed task. The most popular static friction model includes Coulomb and viscous friction and Stribeck effect. Its mathematical model is expressed by the following system of equations [2]:

$$T_f(w) = \begin{cases} \pm T_{brk} : & \omega = 0 \\ \left(T_c + (T_{brk} - T_c) e^{-\left(\frac{\omega}{\omega_s}\right)^2} + T_\omega |\omega| \right) \mathrm{sgn}(\omega) : & \omega \neq 0 \end{cases} \quad (1)$$

One of the static friction's limitations is its discontinuity in the zero velocity point. These models do not specify the process of phenomenon progress in the case of changing direction of a movement (*stick-slip* phenomena), increasing and decreasing of a velocity (*frictional lag*), movement before sliding phase (*presliding displacement*) and dependents friction on position (*hysteresis of friction*) (fig. 1).
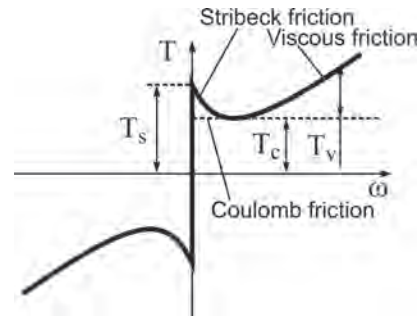

Fig. 1. Static, discontinuous model of friction
Rys. 1. Statyczny, nieciągły model tarcia

The above model is too idealistic due to the discontinuity in zero velocity point. This discontinuity apart from the lack of physical representation introduces difficulties during numerical calculations. This simplification also does not allow us to show sudden changing of friction action direction. To avoid this limitation, very little but finite area of velocity in the nearest vicinity of the zero was introduced. This area determines the linear dependents between velocity and friction (fig. 2). The coefficient of the proportionality is the quotient of the static friction T_s and threshold velocity ω_{th}.

It was experimentally proven, that adopting the value of threshold velocity from the range of 10^{-3} to 10^{-5} ensures the compromise between accuracy and computational effectiveness. Friction torque calculated using the above model does not suppress thoroughly the movement of a driven object, but below threshold velocity causes it to crawl. After introducing the transition area, the static friction model takes the following form [3]:

$$T_f(w) = \\ = \begin{cases} \left(T_c + (T_{brk} - T_c) e^{-c_w |\omega|} \right) \mathrm{sgn}(\omega) + f\omega : & |w| \geq \omega_{th} \\ \omega \dfrac{f\omega_{th} + \left(T_c + (T_{brk} - T_c) e^{-c_w |\omega|} \right) \mathrm{sgn}(\omega)}{\omega_{th}} : & |w| \geq \omega_{th} \end{cases} \quad (2)$$
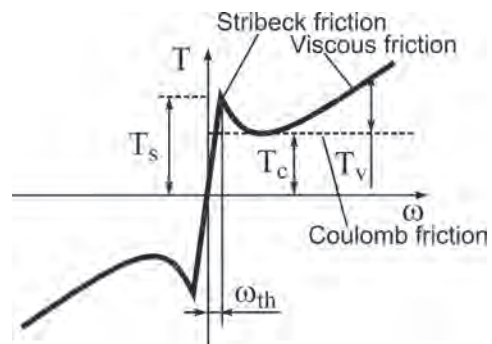

Fig. 2. Static, continuous model of friction
Rys. 2. Statyczny, ciągły model tarcia

The above models do not describe friction dependency on microsliding displacements [4]. It means that in the zero velocity point the friction may not be equal to the zero, and its value may vary in a wide range. Therefore two different areas of friction are taken into account [5]: displacements before sliding movement – *presliding regime* – BL, in which the friction is a function of displacement and displacement in a sliding phase – *gross sliding regime* – EHL, in which the friction is a function of velocity. These issues needed the dynamic adaptation of the friction model to the situation. Therefore, in response to these needs, a wide range of dynamic models were developed such as: Dahl model, Bristle model, Reset integrator, Bliman and Sorine model, Lubricated Contacts model [6]. The most frequently used dynamic friction model is the LuGre model [7]. It describes the structure of contacting surfaces using elastic bristles, which represents points of rough surfaces contacting each other (fig. 3).
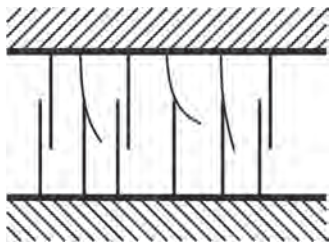

Fig. 3. Dynamic, continuous friction model using bristles
Rys. 3. Dynamiczny, ciągły model tarcia LuGre

LuGre friction model is expressed using the following equations:

$$T_f = \sigma_0 z + \sigma_1 \frac{dz}{dt} + \sigma_2 \omega \qquad (3)$$

$$\frac{dz}{dt} = \omega - \frac{|\omega|}{g(\omega)} z \qquad (4)$$

where z is the average deviation of asperities, σ_0 is the stiffness and σ_1 is the damping coefficient, σ_2 is the viscous damping coefficient whereas the Stribeck effect describes the following equation:

$$\sigma_0 g(\omega) = T_c + (T_s - T_c)e^{-\left(\frac{\omega}{\omega_s}\right)^2} \qquad (5)$$

The LuGre model allows mathematical description inter alia such a phenomenon as friction hysteresis, frictional lag, presliding displacement and stick-slip behavior.

2. Modeling of the driving system

2.1. Static friction model
For the practical reason of stimulating the loading conditions in robot joints it is enough to use the static friction model. Often its application allows for effective realization aims – for example compensation of friction influence on accuracy of positioning. In the paper, the static model friction was used, which modifies common static friction models in a way that allows for better replication of friction characteristics in a robot joint for the whole range of rotational velocity (6) [8].

$$T_j^{(f)} = T_j^{(a,BL)}\, e^{-\left(q_e / q_j^{(s)}\right)^{\delta_j^{(a)}}} + c_j^{(v)}\, \dot{q}_j^{\left(1-\delta_j^{(v)}\right)} \qquad (6)$$

The equation consists of two parts determining the value of friction in the BL area (before the summation sign) and viscotic friction in the EHL area and the way of transition between static to the dynamic friction, called the Stribeck effect. The model contains five unknown parameters; the asperity friction torque $T_j^{(a,BL)}$, the Stribeck velocity $q_j^{(s)}$, the Stribeck velocity Power $\delta_j^{(a)}$, the viscous friction coefficient $c_j^{(v)}$ and viscous friction power $\delta_j^{(v)}$. The parameters $\delta_j^{(a)}$, $\delta_j^{(v)}$ and $q_j^{(s)}$ depend on the configuration of the friction contacts and there are constant values. The parameter $c_j^{(v)}$ depends on the lubricant viscosity and as a result, it depends on the temperature. However, the model in that shape is the discontinuous function, not describing clearly the behavior of the cooperating machine's parts in the case of zero velocity. It has importance due to the possibility of using the model while changing the direction of movement. Therefore further development was proposed. It was solved by introducing inverse tangent function, which smoothes the area of friction transition through the zero velocity (7).

$$T_j^{(f,K)} = \frac{2}{\pi}\arctan(c\dot{q})T^{(f)}\left(|\dot{q}|\right) \qquad (7)$$

Parameter c was used in order to scale the area of changing direction of velocity. Thus, if the changes have to concern the nearest vicinity of the zero it is usually taken the value from the range of -10^{-4} rad/s to 10^{-4} rad/s. In order to obtain this value, the parameter c has to be equal to 10^6.

2.2. Dynamical friction model
For the aim of simulating the influence of friction phenomenon on the robot behavior, the LuGre friction model was used [7]. Block diagram of the model shows the fig. 4.
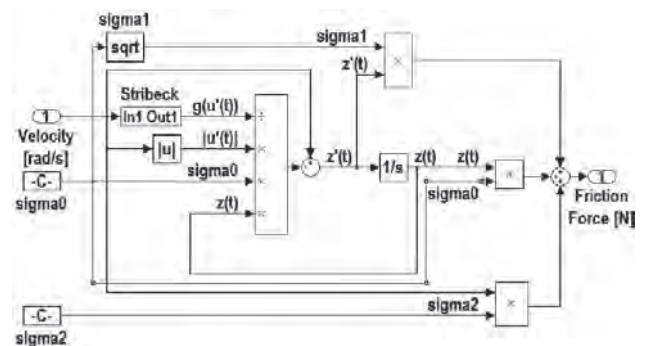

Fig. 4. Block diagram of the dynamical LuGre friction model
Rys. 4. Schemat blokowy dynamicznego modelu tarcia LuGre

During simulations identical values of parameters like in [7] were used (tab. 1).

In order to verify the prepared model the simulation of the formation of friction hysteresis phenomena under the influence of oscillatory force was performed (fig. 5). Ampli-

tude of friction were ± 1.425 N, ± 1.3 N, ± 1 N, whereas frequency of oscillations was 1 Hz, 10 Hz, 25 Hz respectively.

Obtained results were consistent with the literature data.

Table of data	
σ_0	$1 \cdot 10^{-5}$ N/m
σ_1	$1 \cdot 10^{-10}$ Ns/m
σ_2	0.4 Ns/m
T_s	1.5 N
T_c	1 N
ω_s	0.001 m/s

cal gear. It contributed to the correct way of damping both movements of the motor's shaft and the robot arm.

The motor's shaft was connected also with reduced gear's and motor's rotor mass moment of inertia. Thus, the input-output equation for the whole driving system takes the following form:

$$n_3\left(T_{3,ideal} - J_{3,gear}\ddot{\varphi}_3 - T_{3,f}\right) = T_{3,ARM} \qquad (8)$$

Based on the block diagram of the control system (fig. 6) and equation (8) the numerical model of the robot driving system in the third joint was performed (fig. 7).

The model contains masses, mass moments of inertia and a position of mass center of gravity of robot arms and gears and the motor's rotor also. During simulations the values of all above data are assumed to be unknown. It results from the necessity of realistic projections of the measurement process in reality.

Fig. 5. Hysteresis of friction in presliding regime

Rys. 5. Histerezy tarcia w obszarze przedślizgowym

Fig. 7. Numerical model of the third robot joint contains the friction model, mechanical gears model, robot arms and reference signal system and ideal source of movement

Rys. 7. Model numeryczny przegubu trzeciego zawierający model tarcia, model przekładni mechanicznych, człony robota oraz system sygnału zadanego i idealne źródło ruchu

2.3. Model of the driving system in the third robot joint

In order to obtain clear results of simulations, the ideal source of movement was used. Thanks to this, the calculated driving torque of the motor did not contain the effect of noise influence and effect of time delay of the control system. Driving joint contained the model of mechanical gears with ideal ratio equal to $n_3 = 100$ (fig. 6). The model of the joint contains static and dynamic friction models. The friction was connected directly with the motor's shaft before mechani-
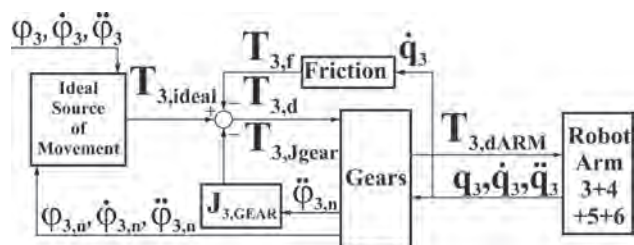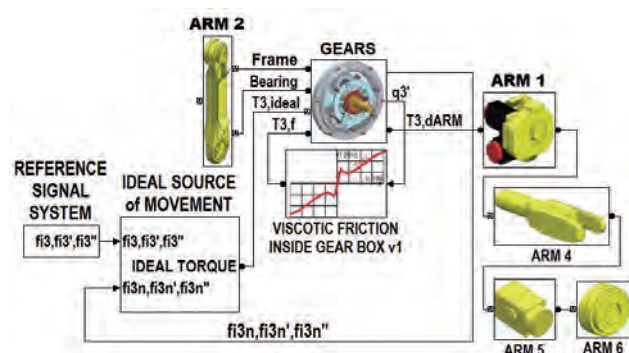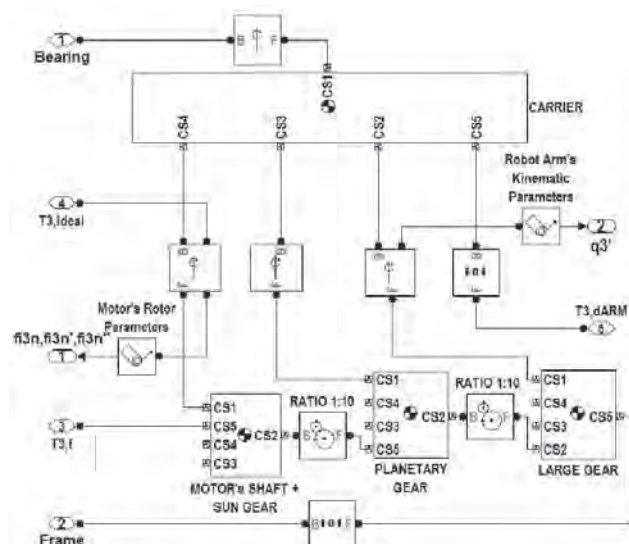

Fig. 6. Input-output block diagram of the robot driving system in third joint

Rys. 6. Schemat blokowy wejścia-wyjścia systemu napędowego robota w przegubie trzecim

Fig. 8. Numerical model of mechanical gears in the third robot joint

Rys. 8. Model numeryczny przekładni mechanicznej w przegubie trzecim robota

3. Friction measurement technique

The investigated subject was the industrial robot FANUC AM100iB. Measured dynamic parameters were the total mass of last four robot arms m_3, the position of its common mass center of gravity $r_{3,x}$, $r_{3,y}$, $r_{3,z}$ and the viscous friction characteristics in the third robot joint. Simulation of robot states based on using the inverse dynamic in order to determine the values of driving torques after setting kinematic parameters of the robot movement (fig. 9).
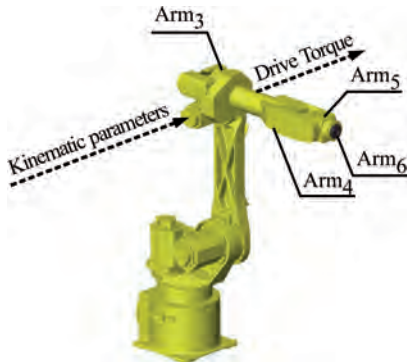

Fig. 9. Investigated object FANUC AM100iB robot
Rys. 9. Badany obiekt robot FANUC AM100iB

To determine the viscous friction characteristic its value had to be extracted from the total, measured driving torque of a motor. This aim leads us to the situation in which the total motor's torque depended on two factors. One of these was reduced torque of gravity force, whereas the second one was viscotic friction torque. This state existed during uniform motion of the driven joint. Then resistive torque of movement, acting on driven arm resulted only from the force of gravity:

$$T_{3,ARM} = m_3 \cdot g \cdot r_3 \cdot \cos\left(q_3^c + q_3\right) \qquad (9)$$

where q_3^c is the constant angular position of the common mass center of gravity for all driven arms in relation to the third robot axis, q_3 is the angular position of the third robot arms. Input-output equation of the whole driving system takes the form:

$$n_3\left(T_{3,ideal} - T_{3,f}\right) = m_3 \cdot g \cdot r_3 \cdot \cos(q_3) \qquad (10)$$

Hence the relationship for the value of viscous friction:

$$T_{3,f} = T_{3,ideal} - \frac{m_3 \cdot g \cdot r_3 \cdot \cos(q_3)}{n_3} \qquad (11)$$

Because in the equation (11) both the mass driven arms and position of their common mass center of gravity r_3 are unknown, therefore their surrogate values were determined.

3.1. Representation of a mass and position of mass center of gravity of robot arms using surrogate values

For the aim of determining surrogate values of the mass and surrogate values of mass center of gravity of robot arms the simulations of measurements loading in the third robot joint
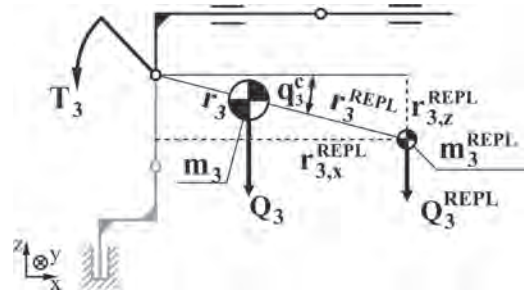

Fig. 10. Phenomenological model of the investigated robot and designation of its kinematic and dynamic parameters
Rys. 10. Model fenomenologiczny robota oraz oznaczenia jego kinematycznych i dynamicznych parametrów

were performed. Phenomenological model of the investigated robot and designation of its kinematic and dynamic parameters shows fig. 10.

Because the mass of all robot arms and their mass centers of gravity are unknown in reality, the representation of their surrogate values was assumed in that form, which ensures obtaining identical values of calculated torque with measured driving torque.

$$m_3^{REPL} = \left| \frac{T_{3,ARM}^Q}{n_3 \cdot g \cdot r_3^{REPL} \cdot \cos\left(q_3^c\right)} \right| \qquad (12)$$

where n_3 is the value of mechanical gears ratio, $T_{3,ARM}^Q$ is the value of gravitational torque, q_3^c is the angular position of real and surrogate mass center of gravity of robot arms, whereas r_3^{REPL} describes distance between the surrogate mass center of gravity and the third robot axis. The value of gravitational torque $T_{3,ARM}^Q$ and angular position of surrogate mass center of gravity had to be determined based on its measurement. The values r_3^{REPL} had to be chosen arbitrarily. Difficulties in application of this equation results from the necessity of performing very accurate measurements and obtaining the full transmission of gravity force onto the motor's shaft. It allows determining the correct value of the gravitational torque $T_{3,ARM}^Q$.

3.2. Determination of angular position of the mass center of gravity of robot arms

In order to determine the angular position of robot arms mass center of gravity the movement of last four robot arms was performed around the third robot axis with low rotational velocity. While moving the third arms, its angular position $\dot{q}_3$, rotational velocity of motor's shaft $\dot{\varphi}_3$ and value of driving torque were measured (fig. 11).

The movement was performed in the way that ensured transition of the mass center of gravity through the point of maximum arm of gravity torque. It corresponds to the horizontal position of mass center of gravity relative to the third robot axis (fig. 12).

In uniform motion the viscous friction torque takes a constant value, whereas changing arm of gravity force acting generates varying value of driving torque. In that way the rough value angular position q_3^c, where the maximum motor's load $T_{3,ideal}^{\max}$ existed was determined (fig. 13).

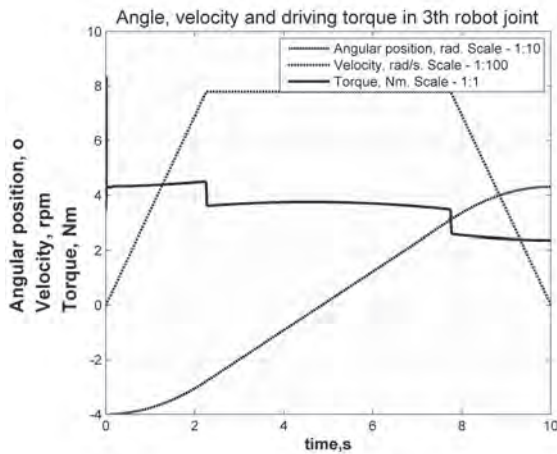The rough value of angular position of the mass center of gravity equals to:

Fig. 11. Kinematic and dynamic parameters of rough movement

Rys. 11. Parametry kinematyczne oraz dynamiczne przejazdu zgrubnego
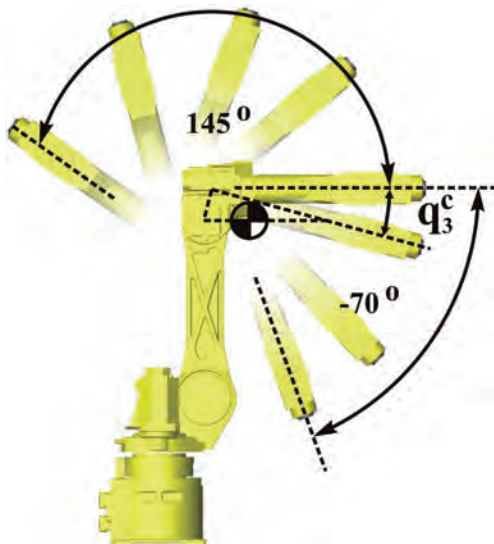

Fig. 12. Available range of robot arms motion and angular position of mass center of gravity

Rys. 12. Dostępny zakres ruchowy robota oraz położenie środka ciężkości ostatnich czterech ramion
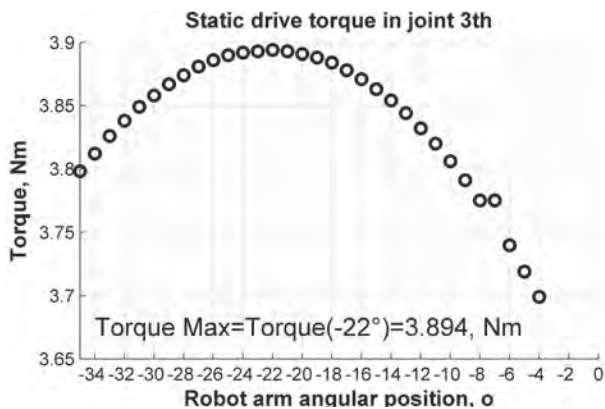

Fig. 13. Rough determination of angular position of the maximum motor's load existence

Rys. 13. Zgrubne określenie wartości kąta występowania maksymalnego obciążenia silnika

$$q_3^c = -22° = 0.383 \text{ rad}$$

In the subsequent step the very precise movement in the nearest vicinity of the previously determined angle was performed. In that way the very precise angle of maximum motor load existence was determined (fig. 14).
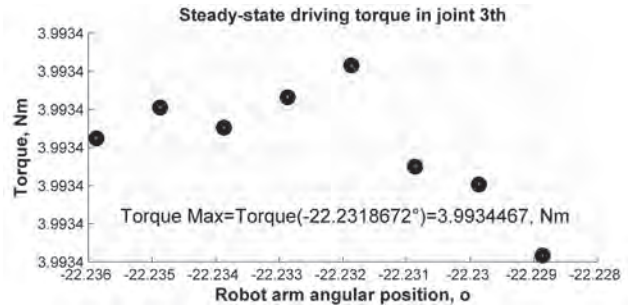

Fig. 14. Very precisely determined angle of the maximum motor's load existence

Rys. 14. Precyzyjne wyznaczenie kąta występowania maksymalnego obciążenia

The precise value of angular position of the mass center of gravity equals to:

$$q_3^c = -22.23187° = 0.38801 \text{ rad}$$

3.3. Analysis of transition the value of gravitational torque onto the motor's shaft

The measured value of the motor's maximum load consisted of the reduced gravitational torque and viscous friction torque:

$$T_{3,ideal}^{\max} = T_{3,f} + \frac{T_{3,ARM}}{n_3} \qquad (13)$$

To determine the value of reduced gravitational torque, it had to be lead to such a state, in which the friction $T_{3,f}$ did not affect the driving torque of the motor. It means that
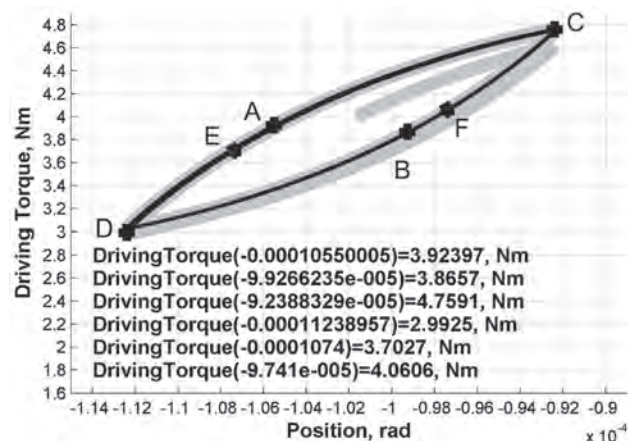

Fig. 15. Hysteresis friction in third robot joint

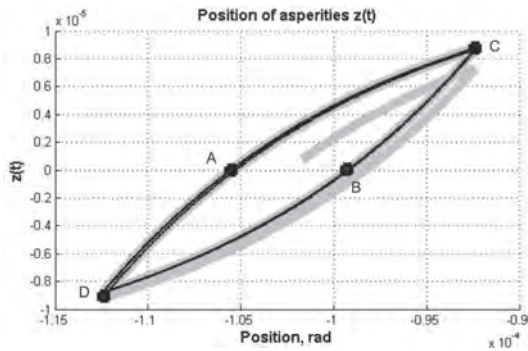**Rys. 15.** Histereza tarcia w przegubie trzecim robota

Fig. 16. Hysteresis of friction asperities position z(t) and robot arms position

Rys. 16. Histereza położenia chropowatości z(t) w stosunku do położenia kątowego ramienia
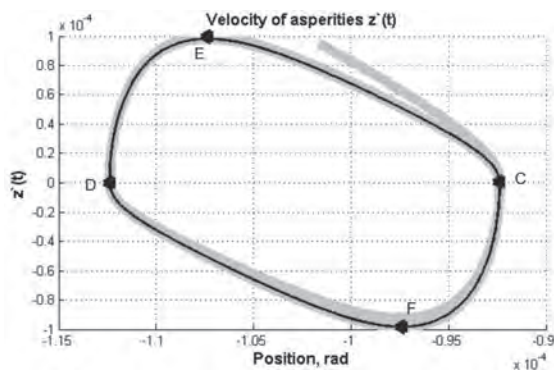

Fig. 17. Hysteresis of velocity of asperities z'(t) and robot arm position

Rys. 17. Histereza prędkości chropowatości z'(t) w stosunku do położenia kątowego ramienia

the full transition of gravity force onto the motor's shaft had to be obtained. According to the static friction models, this situation exists in zero velocity point. But these kinds of models do not describe dynamical friction behaviors in a realistic way in the presliding regime of friction [7]. Therefore, for the purpose of determining the value of driven arms mass, the analysis of dynamical friction phenomenon influence on driving torque in zero velocity point was performed. Experiments rely on the introduction of the robot joint into the angular vibration, relative to the previously determined angular position of existence the maximum motor's load q_3^c. During the vibrating movements, the measurements of kinematic and dynamic parameters of robot arms and motor were performed. Joint movement of the oscillation was driven by the torque, its value depends on angular micro-positions of the arm. The effect of this dependency results from the phenomena of friction hysteresis and presliding displacements. As a result of the experiment the hysteresis plot of friction in the third robot joint was obtained (fig. 15). The hysteresis of friction asperities position and robot arms position (fig. 16) and the hysteresis of velocity of asperities and robot arm position (fig. 17) was also obtained.

Based on plots of hysteresis of position and velocity of asperities, characteristic points of oscillatory movement were determined. Those points correspond to the values of driving torque, read from the hysteresis friction plot. Values of driving torques obtained based on dynamical analysis were used to calculate the set of surrogate masses of robot arms tab. 2.

The value of surrogate distance of mass center of gravity was selected arbitrarily as:

$$r_3^{REPL} = 500 \text{ m}$$

For the purpose of final selection of the correct surrogate mass, the set of viscous friction characteristics were prepared and compared together. All values were calculated based on (11), which was supplemented with successive values of surrogate masses.

3.4. Determination of viscous friction characteristic in third robot joint

Viscous friction characteristics show dependence between the resistive torque of movement and motor's rotor velocity. Determination of viscous friction characteristics relied on repeatedly moving the set of the last four robot arms with increasing velocity. During each movement cycle the measurement of driving torque was performed at the time when the constant velocity was obtained. In the uniform movement, the values of driven torques are equal to the sum of viscous friction and reduced torques of gravitational forces. Determining surrogate masses allowed extraction of the gravitational torque from the total driving torque. For this purpose, during reading values of driving torque the angular position of robot arm were performed. Increased values of rotational velocities, the subsequent values of viscotic

Tab. 2. Selected values of driving torques and surrogate masses correspond to them

Tab. 2. Wybrane wartości momentów napędowych oraz odpowiadające im wartości mas zastępczych

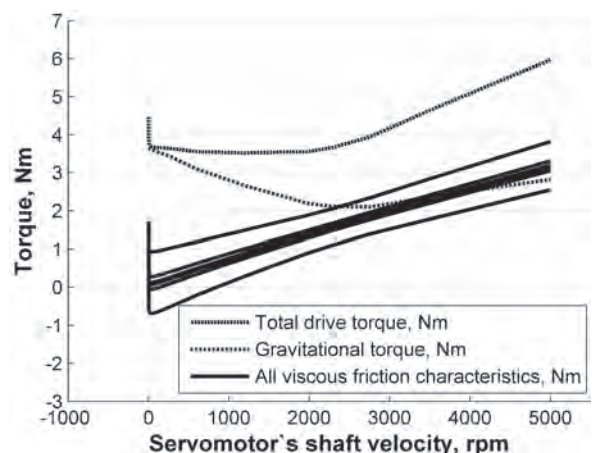| Table of data	
$T_{3,dA} = 3.924$ Nm	$m_{3REPLA} = 79.999$ kg
$T_{3,dB} = 3.866$ Nm	$m_{3REPLB} = 78.811$ kg
$T_{3,dC} = 4.759$ Nm	$m_{3REPLC} = 97.023$ kg
$T_{3,dD} = 2.993$ Nm	$m_{3REPLD} = 61.009$ kg
$T_{3,dE} = 3.703$ Nm	$m_{3REPLE} = 75.494$ kg
$T_{3,dF} = 4.061$ Nm	$m_{3REPLF} = 82.785$ kg

Fig. 18. Viscous friction characteristics

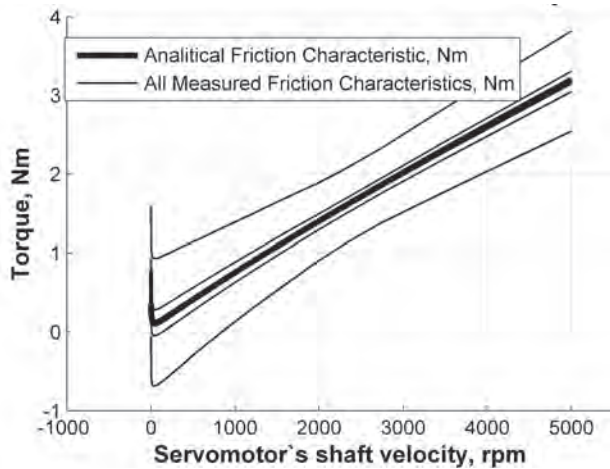**Rys. 18.** Charakterystyki tarcia wiskotycznego

Fig. 19. Viscous friction characteristics

Rys. 19. Charakterystyki tarcia wiskotycznego
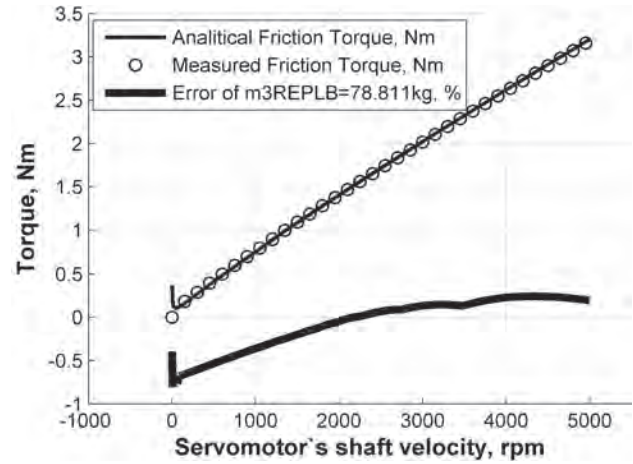

Fig. 21. Selected viscous friction characteristic

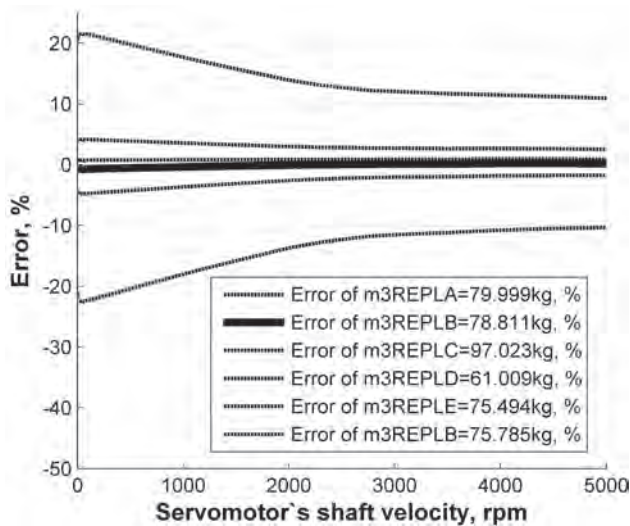**Rys. 21.** Wybrane charakterystyki tarcia wiskotycznego

Fig. 20. Quality assessment of the viscous friction characteristic replication

Rys. 20. Ocena jakości odwzorowania analitycznie wyznaczonej charakterystyki tarcia wiskotycznego

Fig. 22. The choice of the correct value of driving torque and angular position of mass center of gravity

Rys. 22. Wybór właściwego momentu napędowego silnika oraz położenia kątowego ramienia

friction were calculated based on (11). After collecting all measured values of the motor's velocity and corresponding to them values of viscous friction onto one plot, the whole friction characteristics were determined (fig. 18). During uniform movement, the inertia torques do not appear, therefore it was not taken into account. Angular positions of the last three robot arms were constant. It also eliminated the influence of other types of forces.

Characteristics obtained in that way were compared with friction characteristics calculated analytically (fig. 19). Quality assessment of the viscous friction characteristic replication was performed based on the difference between pattern analytical characteristic and determined characteristics of friction. The difference was shown as a percentage of the total driving torque (fig. 20).

Based on the assessment of the error between characteristics, the choice of correct values of surrogate mass was performed as $m_3^{REPL} = 78.811$ kg which correspond to the driving torque equal to $T_{3,d} = 3.866$ Nm. Angular position of
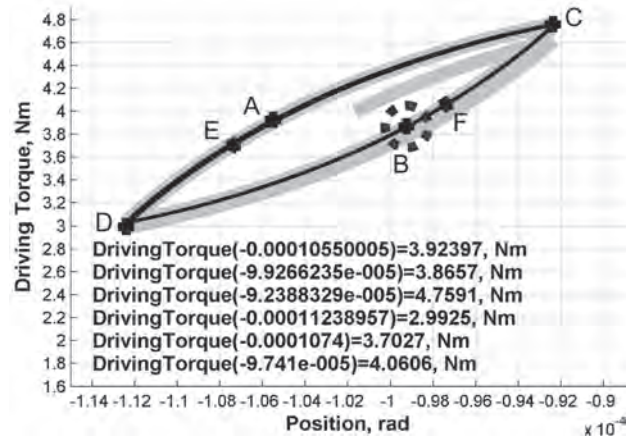
the surrogate mass of gravity equals to the angular position determined during precise movement and less of the value corresponding to that position, in which the above driving torque was selected (fig. 22).

$$q_3^{C,f} = q_3^C - q_3 \qquad (14)$$

4. Conclusion

The obtained results allow us to determine the correct method while performing measurements of the angular position of the mass center of gravity of all driven robot arms and measurements driving torque, comes only from gravitational force. Quality assessment of a viscous friction characteristic replication informs that the measurement of the driving torque coming from gravity force should be performed while dropping the robot arms down during micro-oscillation movements. Additionally the measurement falls at the moment in which the value of asperities z(t) equals to the zero. Thus, it

can be considered, that after determining hysteresis of friction of the real object the driving torque should be measured in the time when asperities changes their position. Existence of zero asperities position should be determined based on hysteresis of friction asperities position $z(t)$ and robot arms position. However, this approach might be difficult to do because of technical limitations. Therefore, for future experiments it is suggested to prepare a method for determining values of all parameters based only on friction hysteresis. The advantage of the proposed approach is not using any *a priori* knowledge and getting the possibility to investigate the dynamic friction phenomenon with full dependence on the robot arms' kinematic and dynamic parameters.

Bibliography

1. Sjoberg J., Zhang Q., Ljung L., Benveniste A., Deglon B., Glorennec P.Y., Hjalmarsson H., Juditsky A., *Nonlinear Black-box modeling in system identyfication: a unified overwiew*, "Automatica", 31, 1995, No. 12, 1691–1724.

2. Canudas de C.C., Olsson, H., Aström K.J., Lischinsky P., *A New Model for Control of Systems with Friction*, "IEEE Transaction on Automatic Control", 40, 1995, No. 3, 419–425.

3. Armstrong B., Canudas de Wit C., *Friction Modeling and Compensation*, The Control Handbook, CRC Press, 1995.

4. Armstrong B., Dupont P., Canudas de Wit C., *A survey of models, analysis tools and compensation methods for the control of machines with friction*, "Automatica", 30, 1994, No. 7, 1083–1138.

5. Swevers J., Al-Bender F., Ganseman C. G., Prajogo T., *An integrated friction model structure with improved presliding behavior for accurate friction compensation*, "IEEE Transaction on Automatic Control", 45, 2000, No. 4, 675–686.

6. Olsson H., Aström K. J., Canudas de Wit C., Gäfvert M., Lischinsky P., *Friction Models and Friction compensation*, "European Journal of Control", 1998, No. 4, 176–195.

7. Canudas de Wit C., Olsson H., Aström K.J., Lischinsky P., *A new model for control of systems with friction*, "IEEE Transaction on Automatic Control", 40, 1995, No. 3, 419–425.

8. Waiboer R.R., Aarts R.G.K.M., Jonker J.B., *Velocity dependence of joint friction in robotic manipulators with gear transmissions*, [in:] *ECCOMAS Thematic Conference Multibody Dynamics, Advances in Computational Multibody Dynamics*, 2005, 1–19. ∎

Metoda pomiaru tarcia wiskotycznego w przegubie robota przemysłowego z zastosowaniem masy zastępczej

Streszczenie: Identyfikacja parametrów dynamicznych robota przemysłowego wymaga stosowania złożonych procedur pomiarowych oraz obliczeniowych. Proces identyfikacji w ogólnej postaci sprowadza się do opracowania modelu matematycznego, który opisuje badany obiekt w sposób ogólny a następie wyznaczane są wartości parametrów tego modelu. W tym celu swoje zastosowanie znajdują różne techniki estymacji, które pozwalają na wyznaczenie parametrów modelu w taki sposób, aby wyniki działania modelu jak najbardziej zgadzały się z wynikami rzeczywistych pomiarów. Powszechnie stosowaną metodą estymacji jest Metoda Najmniejszych Kwadratów. Podczas stosowania tej techniki dynamiczny model robota reorganizowany jest do postaci liniowej. Wówczas wszystkie identyfikowane parametry zestawiane są w jednej macierzy. Umożliwia to zastosowanie algorytmu jednocześnie estymującego wartości wszystkich parametrów. Jest to często proces złożony i czasochłonny ze względu na dużą liczbę pomiarów oraz dużą liczbę parametrów branych pod uwagę. Utrudnia to także badanie dynamicznych zjawisk tarcia w przegubach robota. Autorzy pracy proponują podejście upraszczające proces identyfikacji parametrów dynamicznych robota przez zastosowanie zastępczej masy unoszonych ramion. Wprowadzenie masy zastępczej pozwoli na wyznaczenie charakterystyki tarcia w sposób niezależny od grawitacji i kierunku ruchu a także na obniżenie liczby jednocześnie identyfikowanych parametrów dynamicznych. W celu określenia technicznych możliwości wdrożenia proponowanego podejścia, autorzy przeprowadzili analizę teoretyczną wpływu histerezy tarcia statycznego w przegubie robota na jakość pomiarów. Analizę teoretyczną poparto symulacjami komputerowymi. Podejście to pozwoli także na uniknięcie konieczności stosowania wiedzy a priori.

Słowa kluczowe: tarcie wiskotyczne, pomiar, identyfikacja, przegub robota, symulacja

Prof. Jerzy Świder, PhD, DSc (Eng.)

He received a PhD degree in 1981 from the Silesian University of Technology, DSc degree in 1992 and became a full professor in 2000. He is actually a head of the Institute of Engineering Processes Automation and Integrated Manufacturing Systems and Director of the Congress – Education Center. His scientific interests are mechanics, mechatronics, processes automation, robotics and CAD/CAM systems. He is the author of numerous home and international publications in the field of robotics, mechanics, mechatronics, machine design and operation.

e-mail: jerzy.swider@polsl.pl

Adrian Zbilski, MSc Eng.

PhD student at Silesian University of Technology. Born in1984. Scientific Career: on September 2008 received Msc Eng. degree at Institute of Engineering Processes Automation and Integrated Manufacturing Systems of Faculty Of Mechanical Engineering at Silesian University of Technology. Since November 2008 starts working as the PhD student at Silesian University of Technology on energy consumption of automated machines.

e-mail: adrian.zbilski@polsl.pl